AC Winding Loss of Phase-Shifted Coupled Windings

Ciaran Feeney, *Student Member, IEEE*, Jun Zhang, *Student Member, IEEE*, and Maeve Duffy, *Senior Member, IEEE*

***Abstract*—In circuits where there is an inherent phase shift angle between coupled winding currents such as in coupled inductors, it is important to accurately calculate the ac winding loss at the correct phase shift and frequency. Phase shift between winding currents can cause the ac winding loss to vary significantly due to changes in the magnetic field distribution. This paper presents an analysis of winding loss for the general case of coupled windings with arbitrary phase-shifted currents and its effect in a number of practical devices. A detailed approach to analytically calculate ac winding loss in microfabricated-coupled stripline inductors is presented along with a derivation of the resistance matrix for the device. The analysis and methodology are then validated using finite element analysis and experimental results.**

***Index Terms*—AC resistance, ac winding loss, coupled inductor, gapped transformer, *LLC* converter, microfabricated, phase shift, resistance matrix, resonant converter, stripline, transformer.**

I. Introduction

As the never-ending pursuit of higher switching frequencies and power densities continues unabated [1]–[4], the need for accurate ac winding loss calculation has never been more important. As these trends continue, ac winding losses in magnetic devices are becoming more and more substantial as the thickness of conductors becomes larger than the skin depth of the material. In components where the windings are magnetically coupled, changes in magnetic field distribution due to a phase shift between the winding currents can significantly affect their ac winding loss depending on the skin depth of the conductor and proximity of adjacent windings.

In phase-interleaved coupled inductor windings, the ac winding loss is affected by the phase shift of voltages applied to the windings, which is selected with respect to the number of phases implemented. For example in a three-phase coupled inductor, the windings are driven with a phase shift between the applied voltages of $2\pi/3$ [5]. Consequently, in addition to a phase shift of $2\pi/3$ between fundamental harmonic currents in the coupled phases, the second and third harmonic currents will be phase shifted by $4\pi/3$ and 2π from one another, respectively, and similarly for higher order harmonics. Clearly, the magnetic field distribution in the windings at a phase shift $2\pi/3$ will be considerably different than that at 2π and therefore care must be taken to account for the phase shifts between different harmonic currents when calculating ac winding loss. A difficulty arises when calculating ac winding loss for currents with phase shifts of other than 0 or π due to phase-shifted boundary magnetic fields, which are not accounted for in established equations for ac winding loss.

Ac winding loss in multilayer winding structures is typically calculated by using one of several one-dimensional (1-D) analytical solutions to Maxwell's equations [6–9]. Most of these methods are based on Dowell's formula [6] and are largely dependent on the boundary magnetic fields established by the applied winding currents. However, none of them deal explicitly with the effect of phase-shifted currents on winding loss. Indeed most work in this area assumes that the magnetic fields generated are real with no complex component, as the phase shift between currents in the windings is assumed to be either 0 or π. This assumption will lead to a significant error when calculating ac winding loss when this condition is not met. Some attempts to generalize winding loss calculations in terms of current levels have been made by extracting a resistance matrix [10], but due to the complexity of the boundary magnetic field calculations for individual components of self-resistance, this method is not very widely used and its validity has not been demonstrated for phase-shifted currents. Vandelac and Ziogas present a starting point in the analysis of power loss due to phase-shifted currents [8], for conductors having 1-D magnetic field distributions in the z-direction. However, their model has not been developed or applied to determine the effect of phase shift in practical devices. This paper builds on the analysis in [8] to derive an expression for winding loss caused by phase-shifted currents in foil conductors and identifies that a resistance matrix may be applied to accurately account for the effects of phase shift.

In microfabricated-coupled stripline inductors, where switching frequencies can easily exceed 100 MHz [11], [12], conductor dimensions are often larger than the material skin depth to handle the applied dc current. In these types of closed core structures, where two-dimensional (2-D) magnetic fields are present, implementing a 1-D solution can lead to a significant over estimation of ac winding loss [13], [14]. Previously Wang [14] developed a 2-D analytical method to calculate ac winding loss for microfabricated racetrack inductors in which all winding currents are in phase. This paper builds on that work, providing a method to derive the resistance matrix of microfabricated-coupled stripline inductors and, therefore, an analytical solution to calculate ac winding conduction loss for any arbitrary phase-shifted currents in a coupled stripline inductor.

Transformers inherently have a phase shift between the primary and secondary currents, which is usually assumed to be

Manuscript received November 26, 2014; revised February 5, 2015; accepted March 27, 2015. Date of publication March 31, 2015; date of current version September 29, 2015. Recommended for publication by Associate Editor F. COSTA.

The authors are with the Power Electronic Research Centre, NUI Galway, Galway, Ireland (e-mail: ciaranfeeney5@gmail.com; junzhang.inbox@foxmail.com; maeve.duffy@nuigalway.ie).

Color versions of one or more of the figures in this paper are available online at http://ieeexplore.ieee.org.

Digital Object Identifier 10.1109/TPEL.2015.2418094

negligible; however, this assumption can introduce a significant error when calculating ac winding loss in some cases. In order to demonstrate the scope of the resistance matrix in accounting for phase shift effects on winding loss, two other practical cases are analyzed and validated by Finite Element Analysis (FEA). First, in the transformer of an *LLC* resonant converter, there is a phase shift between the primary and secondary currents due to a magnetizing inductor placed in parallel with the primary side of the transformer, which forms part of the resonant tank to achieve soft switching. In this case, the phase shift changes dynamically with load level [15] and, therefore, for accurate analysis of efficiency, it is paramount to account for phase shift effects in ac winding loss calculations. Also investigated are air core coupled coils, which represent a wireless charging paradigm in which phase-shifted currents are induced due to low-coupling factors.

The remainder of this paper is organized as follows. In Section II, the relationship between ac winding loss and the magnetic field distribution produced by phase-shifted currents is described along with its relationship to the resistance matrix with a detailed derivation provided in the Appendix. Section III details equations for estimating 2-D boundary magnetic field distributions presented in [14] at a phase shift of 0, and also newly developed equations for predicting boundary magnetic fields at a phase shift of π. In Section IV, the magnetic field boundaries are applied to calculate power loss at 0 and π and then used to find the resistance matrix for a coupled microfabricated stripline inductor. Results are compared with FEA simulations, along with a number of typical coupled winding structure cases. In Section V, measurements are presented for a two-layer spiral winding structure typical of those applied in wireless power systems.

II. Modeling of Coupled Winding Resistance

An expression for the ac loss incurred in coupled foils that carry phase-shifted currents may be found by solving for the eddy current distribution $J_y(x)$ produced by the magnetic fields associated with the currents, and applying (1) over the cross-sectional area of each foil, assuming the magnetic field generated has a component in one dimension only

$$P_{\text{loss}} = \frac{1}{2\sigma}\int_0^h \left(J_y(x)\cdot J_y^*(x)\right)dx \tag{1}$$

where σ is the conductivity of the material and h is the foil thickness.

For two parallel foils similar to those investigated by Vandelac in [8] and as shown later in Fig. 8, an expression for total power loss for phase-shifted currents $\underset{\sim}{\boldsymbol{I}}_1$ and $\underset{\sim}{\boldsymbol{I}}_2 = \underset{\sim}{\boldsymbol{I}}_1 e^{j\theta}$ is derived in the Appendix and found to be given by

$$P_{\text{loss,total}} = \begin{bmatrix} \frac{I_1^2}{2\sigma\delta}\begin{pmatrix} \left((a^2+c^2)+(b^2+d^2)\right)F_1(\varphi) \\ -4\,(a\cdot c+b\cdot d)\,F_2(\varphi)\end{pmatrix} \\ +\frac{I_2^2}{2\sigma\delta}\begin{pmatrix} \left((a^2+c^2)+(b^2+d^2)\right)F_1(\varphi) \\ -4\,(a\cdot c+b\cdot d)\,F_2(\varphi)\end{pmatrix} \\ +\frac{I_1 I_2\cos(\theta)}{2\sigma\delta}\begin{pmatrix} (c\cdot d+a\cdot b)F_1(\varphi) \\ -2(a\cdot d+b\cdot c)F_2(\varphi)\end{pmatrix}\end{bmatrix} \tag{2}$$

where a, b, c, and d are constants related to the geometry of foils, δ is the skin depth of the material, and $F_1(\varphi)$ and $F_2(\varphi)$ are hyperbolic functions as defined in (22). Investigation of the first term shows that it accounts for power loss in foils 1 and 2 due to current I_1 flowing in foil 1 only. Simplification of (2) for current flowing only in foil 1 shows that it reduces to a form which represents power loss due to the self-resistance of foil 1, R_{11} given by Spreen [10]. Similarly, the second term may be seen to represent total power loss due to the self-resistance of foil 2, R_{22}.

Analysis of the third term shows that it accounts for loss due to currents flowing simultaneously in both foils, and that the dependence on the phase shift θ between currents is a cosine function. A comparison with the expression for power loss in two windings in terms of a resistance matrix according to Spreen [10] identifies the third term as power loss due to two equivalent mutual resistance terms R_{12} and R_{21}

$$P_{l,\text{total}} = \frac{1}{2}\begin{bmatrix} I_1 & I_2\end{bmatrix}\begin{bmatrix} R_{11} & R_{21} \\ R_{12} & R_{22}\end{bmatrix}\begin{bmatrix} \underset{\sim}{\boldsymbol{I}}_1^* \\ \underset{\sim}{\boldsymbol{I}}_2^*\end{bmatrix}. \tag{3}$$

This can also be written in the form

$$\begin{aligned} P_{l,\text{total}} = {} & I_{1,\text{rms}}^2 R_{11} + I_{2,\text{rms}}^2 R_{22} \\ & + \left(I_{1,\text{rms}} I_{2,\text{rms}} R_{12} + I_{1,\text{rms}} I_{2,\text{rms}} R_{21}\right)\cos(\theta) \end{aligned} \tag{4}$$

for a phase angle of θ between I_1 and I_2. Examination of (2) and (4) therefore confirms that power loss due to phase-shifted currents is accurately predicted in terms of the resistance matrix; i.e., it is generalized in terms of the applied current amplitudes and a cosine function of the phase angle between them.

Depending on the winding structure, the resistance matrix can be found by measurement, by FEA or by solving analytical expressions for the resistance terms based on the magnetic field boundaries. Typically, three test conditions are required to solve the resistance matrix for two or more windings; however, in cases where the windings are identical, it is possible to solve with just two known conditions. This is illustrated for coupled stripline inductors, where expressions for their boundary magnetic field distributions are presented in Section III for currents flowing in phase and out of phase, and these are then applied to determine ac winding loss at an arbitrary current phase shift in Section IV.

III. Boundary Magnetic Fields of Coupled Stripline Inductors

In this section, a microfabricated-coupled stripline inductor shown in Fig. 1 is analyzed. The device, which is designed to operate with a switching frequency of 20 MHz, is assumed to have a winding width, W_w of 34 μm, thickness, W_t of 35 μm, and winding spacing, W_s of 25 μm. The device has a core width spacing, C_{ws} of 10 μm, and the insulation thickness between the core and the top and bottom of the conductor windings, i_t is 4 μm. A $Ni_{45}Fe_{55}$ core surrounds the windings with an assumed relative permeability, μ_r of 280 and thickness, C_t of 4.2 μm. These values are typical for $Ni_{45}Fe_{55}$ applied in microfabricated inductors [16].

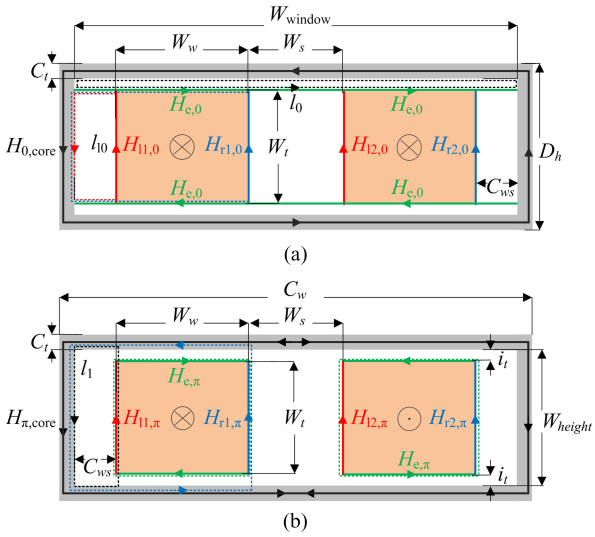

Fig. 1. Cross-sectional views of a coupled microinductor core. (a) Magnetic field intensity boundaries at a phase angle of 0. (b) Magnetic field intensity boundaries at a phase angle of π.

For the structure shown in Fig. 1, the magnitude of the magnetic field intensity within the core is given by

$$H_{\theta,\text{core}} \approx \oint H \cdot \mathrm{d} \cdot l_{\text{mag}} \approx \frac{\underset{\sim}{I}_1 + \underset{\sim}{I}_2}{l_{\text{mag}}} \approx \frac{|I_1 + I_2\,(\cos(\theta) + j\sin(\theta))|}{2(C_w + D_h - 2C_t)} \tag{5}$$

where I_1 and I_2 are the magnitudes of phase-shifted currents flowing in conductors 1 and 2, respectively. It is assumed that the magnetic field is homogenous throughout the core. The core width is C_w, C_l is the core length, C_t is the core thickness, and D_h is the device height. Note that the result can be improved by accounting for the leakage flux due to the free space within the core window, although for most cases this is insignificant.

A. Boundary Field Calculations at $\theta = 0$

The boundary magnetic fields for a phase angle $\theta = 0$ have been described in [14] where current is applied in the same direction in all conductors as shown in Fig. 1(a); their calculation is summarized below for completeness.

The magnetic field intensity at the top and bottom edges of the conductors $H_{\text{e},0}$ can be calculated using the magnetic path l_0 in Fig. 1(a) and Amperes law

$$H_{\text{e},0} \approx -\frac{W_{\text{window}} + 2C_t + 2i_t}{W_{\text{window}}} H_{0,\text{core}} \tag{6}$$

where $H_{0,\text{core}}$ is given in (5) when the phase angle is 0 and W_{window} is the window width.

Taking the magnetic path l_{10}, the boundary field along the left vertical edge $H_{\text{l1},0}$ is given by

$$H_{\text{l1},0} \approx \frac{2C_{ws} \cdot H_{\text{e},0} - W_t \cdot H_{0,\text{core}}}{W_t}. \tag{7}$$

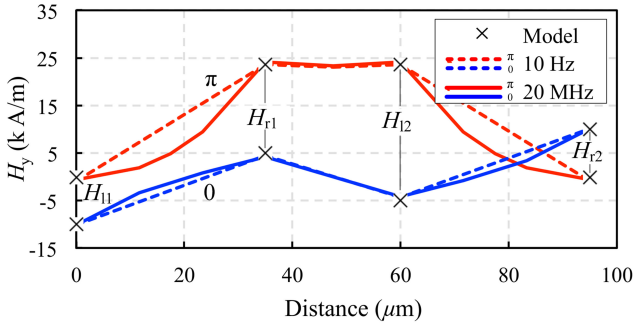

Fig. 2. Vertical magnetic field intensity boundaries of FEA versus model along conductor edges.

Using Ampere's law, the magnetic field intensity along the right vertical edge of the conductor $H_{\text{r1},0}$ is then expressed as

$$H_{\text{r1},0} \approx \frac{2(C_{ws} + W_w)H_{\text{e},0} - W_t \cdot H_{0,\text{core}} + I_1}{W_t}. \tag{8}$$

In the same manner, the magnetic field boundaries for the remaining conductor can be solved.

B. Boundary Field Calculations at $\theta = \pi$

At a phase shift of $\theta = \pi$, the magnetic field distribution in the windings is symmetric about the vertical axis of the structure rather than the horizontal axis as is the case in Section III-A. To estimate the boundary fields, the magnetic path l_1 shown in Fig. 1(b) is followed and calculation commences with the magnetic field intensity along the left vertical conductor edge as

$$H_{\text{l1},\pi} \approx -\frac{W_{\text{height}} + 2C_t + 2C_{ws}}{W_{\text{height}}} H_{\pi,\text{core}}. \tag{9}$$

$H_{\text{core},\pi}$ in this case is estimated as a phase angle of π using (5).

The magnetic field intensity along the right conductor edge is given by

$$H_{\text{r1},\pi} \approx \frac{I_1 + 2(W_w + C_t + C_{ws})H_{\pi,\text{core}} - W_{\text{height}} \cdot H_{\text{l1},\pi}}{W_{\text{height}}}. \tag{10}$$

Then, using Ampere's law, the magnetic field intensity along the top and bottom, $H_{\text{e},\pi}$ of the conductor is defined as

$$H_{\text{e},\pi} \approx \frac{H_{\text{r1},\pi} \cdot W_t + W_t \cdot H_{\text{l1},\pi} - I_1}{2W_w}. \tag{11}$$

This analysis can easily be extended to approximate the magnetic field intensity boundaries for the remaining conductors.

C. Verification of Boundary Field Calculations

Fig. 2(a) compares the calculated magnetic field intensity boundary values described above along the left and right vertical edges of the conductors (shown in Fig. 1) with FEA results. An Eddy current solver within the FEA software package, ANSYS Maxwell [17], was used to analyze a 2-D model of the core described. A maximum error of 0.4% was allowed, with convergence based on loss for this and all FEA simulations hereafter.

Results are plotted as a function of horizontal distance from the left-most conductor edge; i.e., the 0 position is along the boundary $H_{\mathrm{l}1}$. Analysis of two frequencies 10 Hz and 20 MHz and at phase angles 0 (blue) and π (red) show that there is no significant change in magnetic field with frequency at the conductor boundaries, and that the simulated and calculated results are in good agreement. For example, the boundaries $H_{\mathrm{r}1,\pi}$ and $H_{\mathrm{l}2,\pi}$ for a phase angle of π, have an error of approximately 2.3% relative to FEA results. Note that the lines joining the boundary values represent the magnetic field levels in the vertical H_{y} direction only, and are taken along the horizontal center line of the structure shown in Fig. 1.

IV. Modeling and Simulation of AC Winding Loss

An analytical solution for microfabricated-coupled inductor loss at 0 and π is presented using the magnetic field intensity boundaries outlined in Section III and used to derive a resistance matrix for the device. This is followed by an analysis of phase-shifted currents on practical air-core spiral windings and windings within a transformer using a gapped core.

A. Microfabricated Coupled Inductor

Calculating the magnetic field intensities at 0 and π shown in Section III for the structure of Fig. 1, and implementing Wang's equations [14] to find the induced current densities, the power loss in each conductor at phase angles of 0 or π is calculated as

$$P_{l,0/\pi} \approx \frac{1}{2\sigma}\iint (J_{1,0/\pi} + J_{2,0/\pi} + J_{\mathrm{dc}}) \cdot (J_{1,0/\pi} + J_{2,0/\pi} + J_{\mathrm{dc}})^{*} dxdy \qquad (12)$$

where σ is the conductivity of the material, J_{dc} is the dc current density, and $J_{1,0/\pi}$ and $J_{2,0/\pi}$ are current densities induced by the vertical and horizontal flux linkages within the conductors, respectively, at phase shifts of 0 or π. For example, the current density in conductor 1, $J_{1,0/\pi}$ is found using a second-order differential equation derived by Wang [14]

$$J_{1,0/\pi} \approx \upsilon^2 + G \cdot \cosh[\tau x] + Q \cdot \sinh[\tau x] - J_{\mathrm{dc}} \qquad (13)$$

where $\tau = \sqrt{\frac{j\cdot\omega\cdot\mu_0}{\rho}}$, $\upsilon = \sqrt{-\frac{2H_{\mathrm{e},0/\pi}}{W_t}}$, $G = \tau \cdot \frac{H_{\mathrm{l}1,0/\pi} + I_1/W_t - W_w\cdot\upsilon^2 - H_{\mathrm{l}1,0/\pi}\cdot\cosh(\tau\cdot W_w)}{\sinh(\tau\cdot W_w)}$ and $Q = \tau \cdot H_{\mathrm{l}1,0/\pi}$, as defined in [14]. The resistivity of copper is $\rho = 1.7310^{-8}$. The current density in conductor 2, $J_{2,0/\pi}$ can be expressed in a similar fashion.

The total ac power loss is then given for both conductors at a phase shift of 0 and π by

$$P_{l,\mathrm{total},0/\pi} \approx 2P_{l,0/\pi}. \qquad (14)$$

In this analysis, the magnetic field boundaries at a phase angle of 0 are calculated based on the assumption that the $H_{\mathrm{e},0}$ boundary is uniform across the core window; therefore, when calculating the resistance matrix if current is applied to one winding and zero to other, the $H_{\mathrm{e},0}$ boundary would be nonuniform and, thus, would result in a less accurate estimation. Owing to the symmetrical nature of this coupled inductor structure, the resistance matrix can be found using the total power loss calculated previously for a phase shift of 0 and π.

Assuming the self-resistance of each winding is equal and $I_{1,\mathrm{rms}} = I_{2,\mathrm{rms}}$ the mutual resistance R_m can be found by (15). The difference between total power loss at 0 and π is used to estimate the mutual resistance as the power loss due to the self-resistance remains constant. Using this fact it can be deduced that the difference in total power loss is only due to the mutual resistance term

$$R_m \approx R_{12} \approx R_{21} \approx \frac{P_{l,\mathrm{total},0} - P_{l,\mathrm{total},\pi}}{4I_{1,\mathrm{rms}} \cdot I_{2,\mathrm{rms}}}. \qquad (15)$$

It is generally found that the mutual resistance term in this case is negative; however, the total power dissipated in the device is guaranteed to be positive for any winding currents applied since $R_{11}R_{22} > R_{12}^2$.

As the self-resistance terms are assumed to be equal in both conductors, (4) can be simplified and the total loss found at 0 or π can be used to approximate the self-resistance term R_s using R_m as defined by (15). The self-resistance terms are found by

$$R_s \approx R_{11} \approx R_{22} \approx \left[\frac{P_{l,\mathrm{total},0}}{2I_{1,\mathrm{rms}} \cdot I_{2,\mathrm{rms}}} - R_m\right] \approx \left[\frac{P_{l,\mathrm{total},\pi}}{2I_{1,\mathrm{rms}} \cdot I_{2,\mathrm{rms}}} + R_m\right]. \qquad (16)$$

The resistance matrix ***R*** is then expressed as

$$R = \begin{bmatrix} R_{11} & R_{21} \\ R_{12} & R_{22} \end{bmatrix}. \qquad (17)$$

The matrix ***R*** can then be used to calculate power loss when phase-shifted currents are applied to the windings by substituting the matrix values into (4).

Shown in Fig. 3(a) is the implementation of (17) to calculate the ac factor $P_{\mathrm{ac}}/P_{\mathrm{dc}}$, compared with FEA loss results for the structure outlined in Fig. 1, plotted as a function of frequency. The largest discrepancy between FEA results and the model exist when the phase angle is π. This is partly due to the fact that the magnetic field boundaries are assumed uniform along the conductor edges, however, at higher frequencies these become nonlinear, introducing an error into the calculation; most affected is $H_{\mathrm{e},\pi}$ boundary. For instance, at 30 MHz, the skin depth is approximately 2.8 times larger than the winding width which leads to current crowding and, therefore, a change in the magnetic field boundaries.

Fig. 3(b) presents the results of the analytical solution versus FEA results for $P_{\mathrm{ac}}/P_{\mathrm{dc}}$ as a function of phase shift for frequencies of 10 and 20 MHz. There is excellent agreement between the results with a maximum error of 1.7% and 5.2% at 0 and π at 20 MHz, respectively.

B. Other Winding Structures

A two-layer air core coupled winding structure was modeled in which each winding has ten spiral turns on each side of a PCB with an outer diameter of 24 mm, track pitch of 1 mm, track width and thickness of 400 μm and 30 μm, respectively. An axial distance of 400 μm separates the windings. The structure is

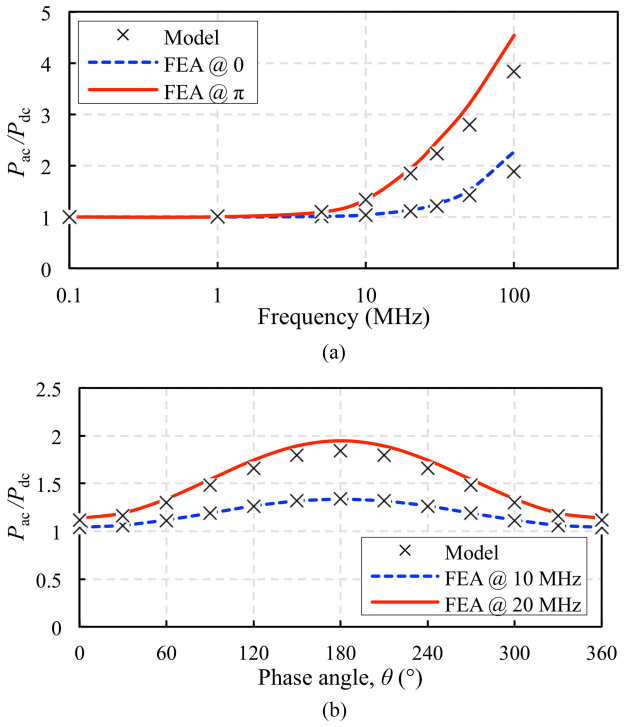

Fig. 3. FEA versus modeled P_{ac}/P_{dc} for a coupled stripline inductor. (a) P_{ac}/P_{dc} at 0 and π. (b) P_{ac}/P_{dc} for varying phase angle.

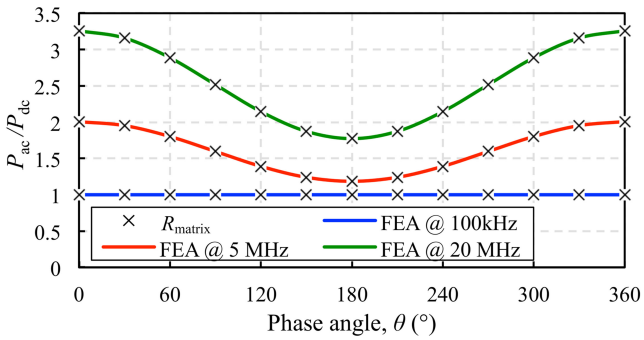

Fig. 4. P_{ac}/P_{dc} of ten turn spiral-coupled windings.

representative of inductive coils used in wireless power systems [18]. In this case, there is no simple analytic solution for the boundary magnetic fields and, therefore, the ac winding loss can be found using FEA, either to calculate a resistance matrix for application in (4) or to vary the phase angle of the applied currents in FEA and calculate the resulting total loss. In this case, as the phase shift between coupled windings varies with load level, application of the resistance matrix in (4) reduces the computational effort required to consider transformer efficiency versus load. Fig. 4 compares the resulting values of P_{ac}/P_{dc}, as a function of phase angle θ using (4) (denoted R_{matrix}) and the FEA results found by varying the phase angle of the applied currents. The resistance matrix is found using the eddy current solver with the same model settings discussed in Section III-C. Each graphed line varies with θ as a cosine function. Clearly, the resistance matrix can accurately represent the total power when the phase angle is varying without the need for multiple simulations.

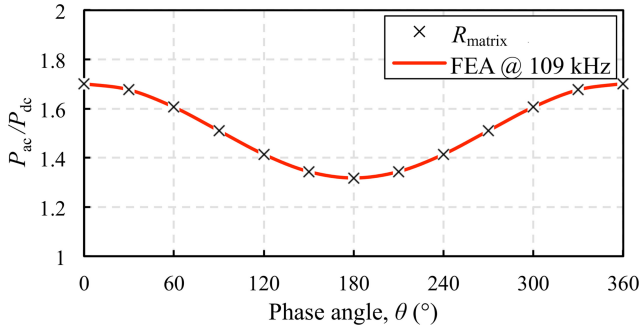

Fig. 5. P_{ac}/P_{dc} of the primary winding in a transformer of an LLC converter.

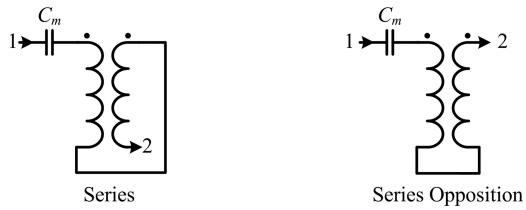

Fig. 6. Connection method of coupled windings for measurement at a phase angle of 0 and π.

As discussed earlier, there is an inherent phase shift associated with transformers used in *LLC* converters. For example, presented in Fig. 5 is the ac factor, P_{ac}/P_{dc} of the primary windings in a planar-gapped transformer described in [19], where, the number of turns on the primary winding and each of the two secondary windings is 35 and 4, respectively. Again, the resistance matrix was found using FEA to produce modeled results of loss versus phase angle presented in Fig. 5 and these are verified with total power loss values predicted in FEA as the phase angle of the applied currents is varied. As in wireless power transfer applications, the use of the resistance matrix greatly reduces computation required to calculate winding losses under different load conditions and, therefore, current phase shifts in *LLC* transformers.

V. Measurements

To illustrate the level of variation between maximum and minimum values of ac resistance, the air-core spiral coupled winding structure described in Section IV-B has been fabricated and tested with phase shifts of 0 and π. The following sections outline the test method and experimental results.

A. Test Method

By connecting the coils in series and series opposition, it is possible to measure the equivalent series resistance at a phase angle of 0 and π, respectively. The inductive reactance of the windings is significant at the frequencies of interest ($f_{sw} \gg 1$ MHz) and this can lead to inaccurate results using an impedance analyzer. To mitigate this effect, a series capacitance C_m is added to reduce the inductive impedance. The capacitance value is selected according to the frequency of interest and coil connection method. Fig. 6 shows the connection method where pins 1 and 2 are the connection points to the impedance analyzer and C_m is the series capacitance.

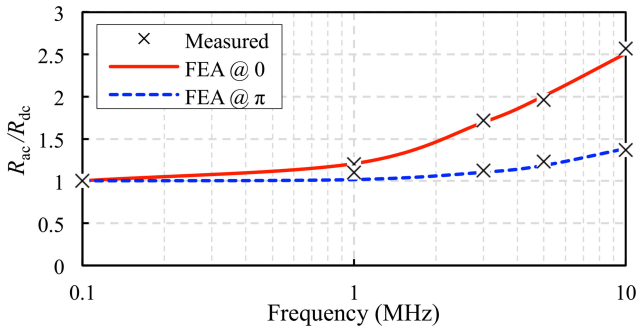

Fig. 7. $R_{\rm ac}/R_{\rm dc}$ of measured versus FEA results at 0 and π for the 10 turn spiral-coupled windings.

B. Experimental Results

Using the test method outlined, an Agilent 4395A impedance analyzer was used to measure the series ac resistance and the results are compared in Fig. 7 with FEA simulation results at phase angles of 0 and π. The dc winding resistance of each winding is 745 mΩ compared to an estimated 604 mΩ predicted using FEA. The error is thought to be as a result of the idealized model implemented in the 2-D FEA simulation model. However, using the resistance factor ratio $R_{\rm ac}/R_{\rm dc}$, the measured and FEA results are in good agreement. At 10 MHz, the measured results deviate from FEA results by 2.3% and 1.3% at phase angles of 0 and π, respectively.

VI. Conclusion

This paper has outlined a method to accurately calculate the resistance matrix for a microfabricated-coupled stripline inductor. This method is useful for the design and optimization of coupled-stripline inductors which are being investigated for PwrSoC applications, as there is no analytical method to calculate ac winding loss incorporating the effect of phase-shifted currents currently available. Incorporating the effect of the phase shift is especially important in these devices when applied in dc–dc converter applications due to the nonsinusoidal phase currents present, which can have a number of significant phase-shifted harmonic currents.

This method assumes that the magnetic field boundaries are uniform along the conductor edges, which in most cases is a reasonable assumption; however, in cases with a low window utilization factor, for example, the flux distribution may be nonuniform, resulting in this method becoming less accurate. Accounting for the nonlinearity of the flux distribution could improve the accuracy of this method.

The use of the resistance matrix has also been demonstrated to accurately account for the effect of varying phase angle for two other magnetically coupled devices where phase-shifted currents are present; i.e., air-core transformers used in wireless power transfer applications and *LLC* resonant transformers. In both cases, application of (4) enables a significant reduction in the level of computation required to investigate the effect varying phase shift has on winding losses under different load conditions. Clearly, the effect of the phase shift can significantly increase winding loss and should be considered as frequencies are extended into the multi-MHz switching frequency range.

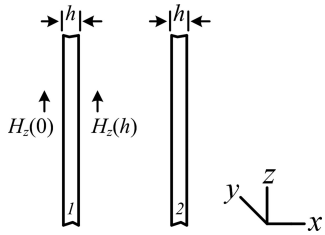

Fig. 8. Two parallel infinitely long and infinitely high foil conductors 1 and 2.

Appendix

Vandelac [8] derived a general expression relating the boundary magnetic fields to ac winding loss for foil conductors. This section develops and applies that expression for two foil conductors that carry sinusoidal phase-shifted currents. It is shown that the resulting loss solves to the same form as that predicted by the resistance matrix.

In Fig. 8, the spacing between the two foils is relatively small and the magnetic field intensity is assumed to be uniform along the z-axis [6]. Since the magnetic field is assumed to be entirely in the z-direction, the Helmholtz equation degenerates to a 1-D problem.

To solve for foil 1, $H_z(0)$ is given as

$$H_z(0) = (\alpha + j\beta) \cdot H_z(h) \tag{18}$$

where $\alpha + j\beta$ is the complex field ratio relating $H_z(0)$ to $H_z(h)$.

Power loss $P_{\rm loss}$ in the y–z plane per square meter can expressed as a function of the magnetic field boundaries across the surface of foil 1 for a sinusoidal wave using [8] by

$$P_{\rm loss} = \frac{H_z^2(h)}{2\sigma\delta}[(1+\alpha^2+\beta^2)F_1(\varphi) - 4\alpha \cdot F_2(\varphi)] \tag{19}$$

where σ is the conductivity of the material, δ is the skin depth of the material, and $F_1(\varphi)$ and $F_2(\varphi)$ are hyperbolic functions

$$\delta = \sqrt{\frac{2}{\omega\mu_0\sigma}} \tag{20}$$

$$\varphi = \frac{h}{\delta} \tag{21}$$

$$F_1(\varphi) = \frac{\sinh(2\varphi)+\sin(2\varphi)}{\cosh(2\varphi)-\cos(2\varphi)}$$

$$F_2(\varphi) = \frac{\sinh(\varphi)\cos(\varphi)+\cosh(\varphi)\sin(\varphi)}{\cosh(2\varphi)-\cos(2\varphi)}. \tag{22}$$

Allowing

$$\begin{aligned} H_z(0) &= a \cdot \underset{\sim}{\boldsymbol{I}}_1 + b \cdot \underset{\sim}{\boldsymbol{I}}_2 \\ H_z(h) &= c \cdot \underset{\sim}{\boldsymbol{I}}_1 + d \cdot \underset{\sim}{\boldsymbol{I}}_2 \end{aligned} \tag{23}$$

where a, b, c, and d are constants related to geometry of the foils. $P_{\rm loss}$ can be expressed in terms of their currents and relative geometries by

$$P_{\rm loss} = \frac{\left|c \cdot \underset{\sim}{\boldsymbol{I}}_1 + d \cdot \underset{\sim}{\boldsymbol{I}}_2\right|^2}{2\sigma\delta}\left[\begin{array}{l}\left(1+\left|\frac{a\cdot\underset{\sim}{\boldsymbol{I}}_1+b\cdot\underset{\sim}{\boldsymbol{I}}_2}{c\cdot\underset{\sim}{\boldsymbol{I}}_1+d\cdot\underset{\sim}{\boldsymbol{I}}_2}\right|^2\right)F_1(\varphi) - \\ 4\mathrm{Re}\left(\frac{a\cdot\underset{\sim}{\boldsymbol{I}}_1+b\cdot\underset{\sim}{\boldsymbol{I}}_2}{c\cdot\underset{\sim}{\boldsymbol{I}}_1+d\cdot\underset{\sim}{\boldsymbol{I}}_2}\right)F_2(\varphi)\end{array}\right]. \tag{24}$$

Power loss, P_{loss} for foil 1 can be expressed in terms of the two applied currents $\underset{\sim}{\boldsymbol{I}}_1$ and $\underset{\sim}{\boldsymbol{I}}_1$ by

$$P_{\text{loss}} = \begin{bmatrix} \frac{1}{2\sigma\delta}\begin{pmatrix} c^2 I_1^2 + 2c\cdot d\cdot I_1\cdot I_2\cos(\theta) + d^2\cdot I_2^2 + \\ a^2 I_1^2 + 2a\cdot b\cdot I_1\cdot I_2\cos(\theta) + b^2 I_2^2 \end{pmatrix} F_1(\varphi) \\ -\frac{2}{\sigma\delta}\begin{pmatrix} a\cdot c\cdot I_1^2 + a\cdot d\cdot I_1\cdot I_2\cos(\theta) + \\ b\cdot c\cdot I_1\cdot I_2\cos(\theta) + b\cdot d\cdot I_2^2 \end{pmatrix} F_2(\varphi) \end{bmatrix}. \tag{25}$$

Simplifying (25), power loss, P_{loss} for foil 1 can be expressed in terms of the currents I_1 and I_2 and the phase angle between them θ

$$P_{\text{loss}} = \begin{bmatrix} \frac{I_1^2}{2\sigma\delta}\left((a^2+c^2)F_1(\varphi) - 4a\cdot c\cdot F_2(\varphi)\right) \\ +\frac{I_2^2}{2\sigma\delta}\left((b^2+d^2)F_1(\varphi) - 4b\cdot d\cdot F_2(\varphi)\right) \\ +\frac{I_1 I_2\cos(\theta)}{2\sigma\delta}\begin{pmatrix} (2c\cdot d + 2a\cdot b)F_1(\varphi) - \\ 4(a\cdot d + b\cdot c)F_2(\varphi) \end{pmatrix} \end{bmatrix}. \tag{26}$$

It is clear that this result takes the same form as the resistance matrix, where the first part represents the power loss in foil 1 due to current I_1, the second part represents the power loss in foil 1 due to current I_2 flowing in foil 2, and the third part represents the power loss in foil 1 due to both currents I_1 and I_2 and their relative phase shift θ.

Following the same methodology, power loss in foil 2 can be described in a similar fashion. The result of combining the power loss for foils 1 and 2 is shown in (2).

ACKNOWLEDGMENT

The authors would like to thank an anonymous reviewer for their helpful comments.

REFERENCES

[1] C. O'Mathuna, N. Wang, S. Kulkarni, and S. Roy, "Review of integrated magnetics for power supply on chip (PwrSoC)," *IEEE Trans. Power Electron.*, vol. 27, no. 11, pp. 4799–4816, Nov. 2012.

[2] A. Knott, T. M. Andersen, P. Kamby, J. A. Pedersen, M. P. Madsen, M. Kovacevic *et al.*, "Evolution of very high frequency power supplies," *IEEE J. Emerg. Sel. Topics Power Electron.*, vol. 2, no. 3, pp. 386–394, Sep. 2014.

[3] C. R. Sullivan, D. V. Harburg, J. Qiu, C. G. Levey, and D. Yao, "Integrating magnetics for on-chip power: A perspective," *IEEE Trans. Power Electron.*, vol. 28, no. 9, pp. 4342–4353, Sep. 2013.

[4] R. Wu and J. K. O. Sin, "High-efficiency silicon-embedded coreless coupled inductors for power supply on chip applications," *IEEE Trans. Power Electron.*, vol. 27, no. 11, pp. 4781–4787, Nov. 2012.

[5] C. Feeney, M. Duffy, N. Wang, S. Kulkarni, and S. C. O Mathuna, "Analysis of coupled microinductors for power-supply-on-chip applications," in *Proc. IEEE Energy Convers. Congr. Expo.*, 2014, pp. 1679–1684.

[6] P. L. Dowell, "Effects of eddy currents in transformer windings," *Proc. Inst. Elect. Eng.*, vol. 113, pp. 1387–1394, 1966.

[7] J. A. Ferreira, "Improved analytical modeling of conductive losses in magnetic components," *IEEE Trans. Power Electron.*, vol. 9, no. 1, pp. 127–131, Jan. 1994.

[8] J. P. Vandelac and P. D. Ziogas, "A novel approach for minimizing high-frequency transformer copper losses," *IEEE Trans. Power Electron.*, vol. 3, no. 3, pp. 266–277, Jul. 1988.

[9] M. P. Perry, "Multiple layer series connected winding design for minimum losses," *IEEE Trans. Power Apparatus Syst.*, vol. PAS-98, no. 1, pp. 116–123, Jan. 1979.

[10] J. H. Spreen, "Electrical terminal representation of conductor loss in transformers," *IEEE Trans. Power Electron.*, vol. 5, no. 4, pp. 424–429, Oct. 1990.

[11] N. Sturcken, E. J. O'Sullivan, N. Wang, P. Herget, B. C. Webb, L. T. Romankiw *et al.*, "A 2.5D integrated voltage regulator using coupled-magnetic-core inductors on silicon interposer," *IEEE J. Solid-State Circuits*, vol. 48, no. 1, pp. 244–254, Jan. 2013.

[12] J. T. DiBene, "A 400 A fully integrated silicon voltage regulator with in-die magnetically coupled embedded inductors," in *Proc. Special Sessions On-Die Voltage Regulators Appl. Power Electron. Conf.* , 2010, Palm Springs, CA, USA.

[13] D. V. Harburg, J. Qiu, and C. R. Sullivan, "An improved AC loss model for the optimization of planar-coil inductors," in *Proc. IEEE 13th Workshop Control Model. Power Electron.*, 2012, pp. 1–7.

[14] N. Wang, T. O'Donnell, and C. O'Mathuna, "An improved calculation of copper losses in integrated power inductors on silicon," *IEEE Trans. Power Electron.*, vol. 28, no. 8, pp. 3641–3647, Aug. 2013.

[15] J. Zhang, W. G. Hurley, and W. H. Wolfle, "Gapped transformer design methodology and implementation for LLC resonant converters," in *Proc. IEEE 29th Annu. Appl. Power Electron. Conf. Expo.*, 2014, pp. 726–731.

[16] N. Wang, T. O'Donnell, S. Roy, P. McCloskey, and C. O'Mathuna, "Micro-inductors integrated on silicon for power supply on chip," *J. Magnetism Magn. Mater.*, vol. 316, pp. e233-e237, 2007.

[17] ANSYS. (2013). *Maxwell 3D (14.1 ed.)*. [Online]. Available: http://www.ansys.com

[18] Y. P. Su, L. Xun, and S. Y. R. Hui, "Mutual inductance calculation of movable planar coils on parallel surfaces," *IEEE Trans. Power Electron.*, vol. 24, no. 4, pp. 1115–1123, Apr. 2009.

[19] J. Zhang, W. G. Hurley, and W. H. Wolfle, "Design of the planar transformer in LLC resonant converters for micro-grid applications," in *Proc. IEEE 5th Int. Symp. Power Electron. Distrib. Generation Syst.*, 2014, pp. 1–7.

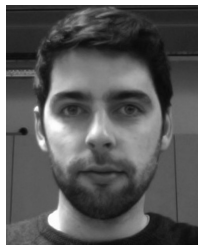

Ciaran Feeney (M'13) received the B.S.E.E. in electronic engineering from National University of Ireland (NUI), Galway, Ireland, in 2011. He is currently working toward the Ph.D. degree in the area of microfabricated inductors for power supply on chip applications in NUI Galway.

He has coauthored a number of publications involving the design of microinductors and their implementation in high frequency dc–dc converters. His interests include high frequency dc–dc converter design, light-load efficiency improvement techniques, and high-frequency magnetic component design.

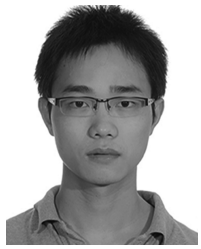

Jun Zhang (S'13) received the B.S. and M.S. degrees in electrical engineering from the Department of Electrical Engineering, Zhejiang University, Hangzhou, China, in 2008 and 2011, respectively. He is currently working toward the Ph.D. degree in the Power Electronics Research Centre, National University of Ireland Galway, Galway, Ireland.

His research interests include high-frequency resonant converters and planar magnetics.

Maeve Duffy (SM'09) received the Graduate and Ph.D. degrees in electronic engineering from the National University of Ireland (NUI), Galway, Ireland, in 1992 and 1997, respectively.

From 1997 to 2001, she was a Research Assistant with PEI Technologies at the NMRC (now Tyndall National Institute) in Cork, Ireland, where she worked on several European and industry funded projects focused on planar magnetics for power electronic applications. Since then, she has been a Lecturer in electrical and electronic engineering at NUI Galway, and she carries out her research in the Power Electronics Research Centre. She has published more than 70 peer reviewed journal and conference papers in the areas of magnetic component design and power electronics. Her current research interests include magnetic component modeling and design for microprocessor loads, energy harvesting, and wireless power systems.